THE ASTRONOMICAL JOURNAL VOLUME 86, NUMBER 3 MARCH 1981

FOCAS: FAINT OBJECT CLASSIFICATION AND ANALYSIS SYSTEM

J. F. JARVIS[a)]
Bell Laboratories, Holmdel, New Jersey 07733

J. A. TYSON[a)]
Bell Laboratories, Murray Hill, New Jersey 07974
Received 18 August 1980; revised 17 November 1980

ABSTRACT

A system for detecting and classifying images on astronomical plates is described. The most fundamental set of data produced using this system to process KPNO 4-m plates of 12 selected areas—number counts as a function of magnitude—is presented. In particular, the very faint and barely resolved images of 24th-mag galaxies are shown to be detectable and distinguishable from stellar images of similar brightness. The algorithms and other implementation considerations used in the construction of the Faint Object Classification and Analysis System (FOCAS) are given. Detection and classification to 24th mag are achieved with nitrogen-baked presensitized IIIa-J plates exposed for one hour in the KPNO 4-m telescope prime-focus camera. For a digital 6000×6000-pixel image made from the central square area 37′ on a side, an average of 7170 objects are found to 24th mag. Since the resulting catalog of objects is 3 to 4 mag deeper than existing surveys, a variety of internal and external tests must be used to assess the accuracy and completeness of the list of objects. The tests and simulations made to support these claims are also discussed.

I. INTRODUCTION

Catalogs, systematic collections of astronomical object descriptions satisfying specified selection criteria, are a fundamental part of observational astronomy. In any statistical astronomical study, it is necessary to investigate properties of images over many magnitudes using the same detection and analysis system. Otherwise, one is open to potentially devastating and subtle systematic errors arising from a variety of causes: detector differences (different color systems), differing sample selection effects, effects due to variations in reduction and analysis techniques, etc. Studies which would immediately benefit from an automated detection and classification system of wide dynamic range include galaxy morphology studies, galaxy-galaxy N-point correlations, galaxy and star number counts, and various other studies as a function of magnitude, color, and galactic coordinates.

In common with many other endeavors, catalog construction can be automated by the appropriate computer technology. This is not a novel observation, since many systems with similar motivation have been described (Herzog and Illingworth 1977; Pratt 1975; Kibblewhite 1975; Lorre 1979; Oemler 1976; Benedict and Shelus 1979; Kron 1979). However, none of these systems are capable of both detecting and classifying objects near the faint limit of photographic plates and simultaneously correctly processing the brightest images that are found even in quiet fields. This paper will describe a system (FOCAS) with a dynamic range of more than 14 mag for the assembly of catalogs of faint objects, both stars and galaxies, from conventional photographic plates. In FOCAS the surface brightness selection threshold is low enough to allow detection of objects with a total magnitude approaching $J = 25$. Normally, only objects brighter than 24th mag are kept in our catalogs because of both increased contamination from noise that becomes increasingly evident dimmer than this limit and incompleteness due to a finite surface brightness detection threshold. The benefits derived from automating catalog construction include the ability to process large numbers of objects, on the order of 10^5; consistent application of selection criteria; and the ability to make exhaustive searches for *all* objects satisfying the selection criteria. Completeness in a catalog is especially important, because much of the desired analysis is statistical.

The specific goals to be met by FOCAS include a faint object detection threshold sufficiently fainter than 24th mag that a magnitude-limited sample at $J = 24$ can be prepared; reliable classification of all objects as stars, galaxies, or noise; the establishment of an apparent magnitude scale; an accurate position for each object; and a characterization of the image shape. Noise is any nonastronomical image such as lint, dust, or artifacts on the plate, as well as images of asteroids, satellites, and meteors. The ultimate limit on sensitivity is the texture in the grain structure of the emulsion which establishes a lower limit to the detection threshold. An apparent

[a)] Visiting Astronomers, Kitt Peak National Observatory, which is operated by the Association of Universities for Research in Astronomy, Inc., under contract with the National Science Foundation.

 0004-6256/81/030476-20$00.90

TABLE I. Summary of observations.

Plate	UT	b^{II}	l^{II}	α(1950)	δ(1950)	Counts to $J = 24$ Galaxy	Star
1286	74 19 Oct	−46.2°	111.1°	$00^h14^m53^s$	+15°36′08″	5251	3335
1561	75 4 Apr	85.6°	64.7°	$13^h06^m15^s$	+29°39′01″	6085	1556
2334	77 14 Mar	75.0°	191.8°	$11^h42^m52^s$	+31°50′27″	4823	2662
2343	77 15 Mar	73.8°	103.4°	$13^h19^m05^s$	+42°50′57″	5841	3577
2345	77 15 Mar	27.1°	111.4°	$18^h45^m39^s$	+79°43′10″	5205	3098
2739	78 3 Feb	27.3°	140.0°	$07^h02^m48^s$	+74°54′17″	3756	2707
2740	78 3 Feb	44.7°	174.4°	$09^h17^m51^s$	+45°51′44″	4161	1593
2741	78 3 Feb	48.7°	188.4°	$09^h36^m50^s$	+36°07′34″	5051	1685
2742	78 3 Feb	78.2°	188.0°	$11^h58^m25^s$	+31°50′02″	6213	1538
2743	78 4 Feb	−34.5°	164.1°	$03^h07^m11^s$	+16°54′29″	5650	1651
2747	78 4 Feb	67.1°	184.8°	$11^h08^m47^s$	+35°57′03″	4756	1351
2766	78 4 Mar	60.0°	160.3°	$10^h59^m33^s$	+44°43′17″	3209	1307

magnitude is essential for each object, for this enables direct summarization of results of different plates and also because it is a much needed parameter in the eventual analysis of the data. In addition, instances of two or more object images that overlap should be detected and the images separated. On the output side of FOCAS, a very general and practicable object selection facility is needed to allow ready access to selected subsets of the data in the catalog.

An important constraint on the design of the system was that existing image digitization and computing resources be used in its implementation. Plates are digitized to a 6000 × 6000-pixel digital image using a 20-μ aperture on the KPNO PDS scanning microdensitometer. FOCAS is a collection of programs written and executed originally on the DEC PDP-11/45 and now on the VAX 11/780 computers controlled by the UNIX* operating system (Ritchie and Thompson 1974). In addition to the standard peripherals, a medium-resolution color raster graphics display system is also available. This display is invaluable for both algorithm development and analysis of the data.

FOCAS is composed of several major components for performing the following functions: object detection, classification, and object list (catalog) manipulation. Reducing a digitized plate image to a list of unclassified objects (detection) is typically a 12-hr job on the 11/45. Following this, an interactive, two-stage procedure is performed to classify each object as one of the three possible types: noise, stars, or galaxies. This represents an application of conventional nonparametric statistical pattern recognition techniques. Once classification is accomplished, various subsets of the object list can be selected for input to analysis routines.

For N_2 presensitized Kodak IIIa-J plates and a one-hour exposure at high galactic latitudes on the KPNO 4-m telescope, approximately 16 000 objects per plate are found that meet the detection criteria. The $J = 24$ magnitude-limited sample averaged over all 12 plates after correcting for offset guide pellicle shadows and telescope nonlinearities (Chiu 1976) is 19 200 objects per square degree. Summarizing, a catalog is a set of computer files, normally associated with a plate on a 1:1 basis containing a description of the objects found on the plate. These files contain a header with the usual plate specific information as well as an entry for each object. Selection programs allow specification of objects for inclusion in output lists by intrinsic parameters (magnitude, type) or by plate-related data (galactic coordinates).

The programs (all statistical in nautre) now being undertaken include analysis of the object counts as a function of type, magnitude, and galactic coordinates; an analysis of galaxy clustering phenomena through application of correlation techniques; faint-cluster detection; and a study of gravitational lens distortions of background galaxy images. The galaxy and star count data will be presented and discussed in this paper. A paper describing some preliminary results of the number count analysis has been published (Tyson and Jarvis 1979).

II. OBSERVATIONS AND DATA

Plates selected for analysis by FOCAS were chosen from the best seeing plates (stellar diameters <1.5 arcsec) taken over the past four years for two of our programs on the Mayall 4-m telescope at Kitt Peak National Observatory. Many of these plates, which were taken at various latitudes, were centered on a single foreground galaxy (typically 18th mag). Another selection criterion is that the sky diffuse density must exceed 0.6 so that faint objects are well within the linear portion of the γ curve. The final selection criterion is the absence of bright objects in the field. Star images brighter than approximately 7th mag and galaxy images brighter than approximately 12th mag exceed various internal size limits in FOCAS. Table I lists the plates used in this study, although additional plates of some of these fields are used in tests described in Sec. VI. The plates were similarly sensitized, exposed, and developed: fog ≈ 0.3 density, IIIa-J nitrogen baked, exposed 45 to 75 min at prime focus, UBK-7 corrector, and developed 5 min at 20° C in D19. Projected calibration spots were used, with the step wedge and a 0.8-mm aperture. The plates were digitized in 20-μ (0.37 arcsec) steps with a 20-μ-square aperture (pixel) in a raster of 6000 × 6000

* UNIX is a trademark of Bell Laboratories.

pixels, with a scanning time of 7 hr. In each case the microdensitometer bias was zeroed on the plate fog. The 12-cm-square area scanned corresponds to a field 37′ on a side for plates exposed in the KPNO 4-m telescope prime focus camera. The plates were adjusted so that the entire plate was in good focus on the PDS microdensitometer and the vignetted area of the offset guide pellicle was outside or only minimally intruded into the digitized square. The plates were scanned in one continuous session in four sequential rectangular rasters, creating four tapes per plate. Digitized image areas containing the transition from one raster to another were carefully examined for drift in position or density. No drifts were detected in position and none in density were large enough to interfere with the object detection process. Rasters centered in at least 12 of the calibration spots were also digitized. At every point in the processing and handling of the plates, care was taken to minimize lint and dust contamination.

Some of our studies require color information and more widely spaced galactic longitude samples. Thus our observing is continuing, overlapping in several cases with areas photographed and studied by others (SA 57, SA 68).

III. PROCESSING A DIGITIZED PLATE TO A LIST OF OBJECTS

The problem, simply stated, is to reduce a 6000 × 6000-pixel image to a list of objects. This list will include for each object, the magnitude, position, and all features required for the subsequent classification for objects ranging in magnitude from fainter than 24th to the brightest objects in each field. Particular care has been taken to ensure that all bright objects, both stars and galaxies, have been correctly processed in order to allow comparisons with existing surveys made to brighter limiting magnitudes.

The basic digital image generated on the PDS microdensitometer comes as a set of four standard 800-BPI magnetic tapes. A pixel is an 11-bit density value coded as two 6-bit characters. Each tape set also includes small areas scanned on 12 of the 16 intensity calibration spots projected on the plate by the KPNO 4-m prime focus camera. The main image is reduced to an 8-bit/pixel representation on two 800-BPI tapes by a nonlinear mapping of the 11-bit density values to 8-bit representations. The mapping typically resolved the background sky density at the equivalent of a 9-bit resolution, at which point the rms value of the sky density in areas containing no detectable objects is greater than the density quantization step size.

The initial plate-processing step is to generate a representation of the emulsion characteristic curve from the calibration spots using Eq. (1) of Tsubaki and Engvold (1975). The sensitometer spots are subjected to the same nonlinear mapping as the main image, thus the generation of the characteristic curve compensates for the nonlinear 11-bit to 8-bit transformation. Determination of the characteristic curve enables conversion of plate density values to intensities, thus to a magnitude within an additive constant (zero-point J_0). This constant, which is required to establish an apparent magnitude scale, is obtained by processing the images of one or more galaxies or stars that have photoelectric known magnitudes and are dim enough that the emulsion has not reached saturation in the core region. One or more 480-line × 640-column subimages from the full plate containing the calibration objects is processed as the second step of the plate calibration procedure to obtain this constant. The subfield processing runs also enable a reasonable value of the detection threshold parameter to be set. In particular, it is chosen so the selection due to surface brightness limitations occurs at $J \geq 24.5$ mag.

a) Segmentation

The object detection process is dominated by three major considerations. First, to ensure apparent magnitude selection at $J \leq 24.5$, objects with a peak surface brightness of about 3% of the sky brightness must be detected. Such objects have significant surface brightness down to about 26th mag per square arcsecond, which causes a density change approximately equal to the rms value of the density evaluated in areas not containing an object. Second, owing to nonuniform illumination by the telescope and UBK-7 corrector, the sky density changes by about 20% from the center to the edges of the square areas scanned. Third, the processor limits the detection phase to a maximum of five lines of the image in the fast (core) memory.

Detection is accomplished by comparing the average density computed in a 5 × 5 array of pixels (box filter) to the local sky density value. If this value is greater than the sky value by a specified threshold, the pixel is taken to be part of an object. If the threshold is not exceeded, the resulting average value is used to update the local sky value estimate. Thus, sky density values which are kept on a reduced resolution grid are effectively generated by a low pass filter. The object detection operation proceeds along a line allowing the use of run length codes to represent segments brighter than the local sky. The run length code is simply the starting and stopping indices of a contiguous part of a scan line whose brightness is greater than the local sky value by the threshold value. In addition, as the image is scanned, a series of reduced-resolution images (5:1 usually) and a sky density image (16:1 linear reduction) are also prepared. The low-resolution plate images are used by an interactive program that allows review of the entire segmentation and classification process. While more optimal filters could be used in the detection step, the limited computational capability of the 11/45 effectively rules this out. The segmentation process using the 5 × 5 box filter consumes about 40% of the total computer time accu-

mulated during the plate to object list processing. Tests consisting of matching objects by processing two plates of the same field indicate the 5 × 5 filter detects 97% of objects brighter than 24th mag. A second test, processing computer-created fields of dim stars, indicates the 5 × 5 filter maximizes the ratio of the number of real objects to noise objects when compared to 3 × 3 or 7 × 7 detection filters.

b) *Area Assembly*

The second step in the image analysis procedure is to correlate the individual run length codes in the vertical direction into descriptions of object areas. A data structure is created that contains an entry for each line in each image area. This process merges two (or more) runs on a given line when they are both overlapped by a common run on an adjacent line. When nothing is added in the current line to an area description, the assembly of runs into an area description is complete and, if the area exceeds a specified minimum size, it is assumed to correspond to an object of interest and its description is passed to the evaluation routine. The boundary of this area corresponds to the limiting isophote of the detection process, typically 26.5 mag/arcsec^2. A histogram of area sizes is accumulated and is printed at the termination of the plate-reduction run. The area histogram is useful information when specifying the object minimum size threshold.

c) *Object Evaluation*

The third and final step of the basic image to object list reduction is to calculate the various parameters that characterize the individual images in the segmented areas. All quantities are evaluated and if certain consistency checks are satisfied, the object description is put on the output list.

If the area of the object is less than a specified size, 45 pixels, it is replaced by a disk covering 69 pixels. The 69-pixel disk has an equivalent diameter of 3 arcsec or about 3 seeing disk diameters. If the area is greater than this threshold, it is grown radially, increasing the total area by approximately 20% (Fig. 1). The rationale for this procedure is that only part of an image will be detected because of the finite surface brightness threshold that must be exceeded. Enforcing a minimum area for object evaluation, with the minimum dimension related to the seeing disk size, or growing the area by a percentage ensures that the majority of the apparent surface brightness greater than 27 mag/arcsec^2 is included in the area processed. The object area in pixels, after modifications, is included in the output list but is of minimal value for classification or analysis because of these processing steps.

The maximum extents of the object are determined and a rectangular area is defined enclosing it (Fig. 1). The sky density d_s is evaluated in the periphery of this rectangular area, which is separated by a guard area from the central object.

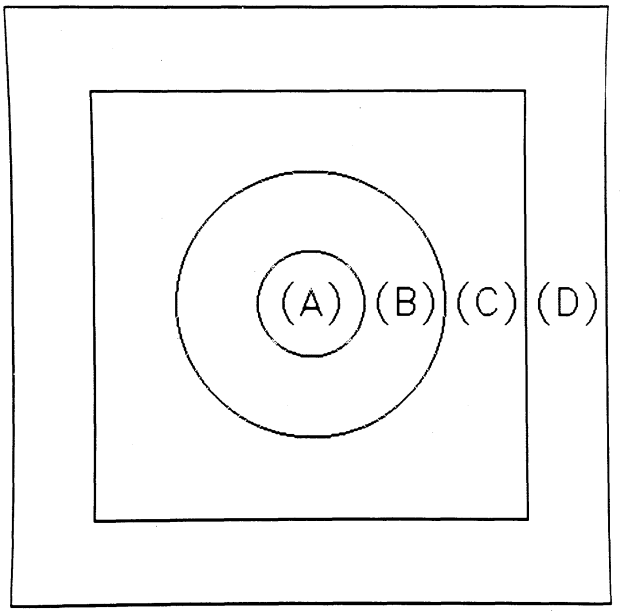

FIG. 1. The relationship of an object area to the image area used to compute the sky density: (A) object area after segmentation; (B) object area after growing process; (C) guard region to minimize object luminosity on sky density; (D) area used to compute sky density.

Accurate determination of the sky density at the location of an object image is a critical step in the object evaluation, since the magnitude and shape discrimination parameters are computed from the difference between the measured densities and the sky density. For example, at 24th total apparent magnitude the difference between the measured total luminosity and the sky luminosity contribution is about 4%. This small difference represents the actual luminosity of the object.

The method used to estimate the sky density is to tabulate a histogram of pixel values in the rectangular band surrounding the object. The mean of the distribution is computed, and a final mean is computed from sky values within ±3 times the rms noise for object-free areas of the plate of the originally computed mean.

If the distribution in the sky determination region is assumed to be slightly skewed owing to contamination from other objects or from luminosity of the central object below the detection threshold, the mode of the distribution would be theoretically more appropriate than the mean. There is a simple method for estimating the mode given the two easily computed quantities, mean and median (Kendall and Stuart 1977). This method involves a subtraction, thus the mode will be noisier than the mean. Simulations and careful evaluation of actual data indicate that the mean based on a truncated distribution is most adequate for this application.

Once the final area corresponding to an object image is determined, the individual parameters or features that will be calculated from the image can be evaluated. In

TABLE II. Summary of plate photometry.

Plate	Seeing	J_0	Reference	Remarks
1286	1.0	28.40	Kron (1979)	21 stars
1561	1.1	27.97	Kron (1979)	15 stars
2334	1.6	28.48	Saslaw *et al.* (1978)	3C 265 + 2 companions
2343	1.4	28.82	Sandage (1972)	3C 285 + QSO + object
2345	1.3	28.49	Sandage (1972)	3C 390.3 + second galaxy
2739	1.1	29.10	Tyson (1979)	2 objects
2740	1.5	29.01	Sandage (1972)	3C 219
2741	1.4	28.71	Sandage (1972)	3C 223
2742	1.3	29.06	Sandage (1965)	3C 268.2 + second galaxy
2743	1.3	28.78	Sandage (1972)	3C 79
2747	1.5	28.97	Tyson (1979)	4 objects
2766	1.2	28.95	Tyson (1979)	2 objects

the following equations $I(x,y)$ is the intensity corresponding to the density at location (x,y) in the digital plate image. Similarly, I_s is the intensity corresponding to the average plate density at the object location. Conversion of the sky density is accomplished directly from the characteristic curve equation. In order to minimize program execution time, conversion of individual pixel density values to intensity is done by table lookup from a table initially prepared from the characteristic curve equation.

The primary computational technique used in characterizing individual objects is the evaluation of the moments of the intensity (Hu 1962). The location of the object is defined by the centroids:

$$\bar{x} = \frac{1}{M_{00}} \sum_A x_i [I(x,y) - I_s], \quad (1)$$

$$\bar{y} = \frac{1}{M_{00}} \sum_A y_i [I(x,y) - I_s], \quad (2)$$

where M_{00}, the zero moment, is

$$M_{00} = \sum_A [I(x,y) - I_s]. \quad (3)$$

In this and following equations summation over A means the sum includes all pixels in the object defining area, A. The apparent magnitude is given by

$$J = J_0 - \log_{2.51} M_{00}. \quad (4)$$

The magnitude scale normalizing constant J_0 is determined from (4) and a measured photolectric magnitude value for at least one faint galaxy or star. The calibration sources and J_0 values for each plate are tabulated in Table II. J_0 is a qualitative indicator of the stability of the magnitude processing since the calibrations determine system gain only to within a multiplicative constant. The magnitude scale used in the current projects is the B_3 scale (Schweizer 1976), usually labeled the J scale. All magnitudes quoted in this paper are on this scale. The particular magnitude scale used is defined by the plate characteristics and the magnitude scale of the calibration galaxies and is not inherent in FOCAS. Calibration galaxies and stars employed have ranged in brightness from 22.5th to 16th mag. A program using the color graphics display system shows the results of the segmentation operation and allows photometry of selected objects with circular apertures of specifiable size. This is an important step in relating FOCAS magnitudes to our observed photoelectric or other published values, usually made through a circular aperture rather than as isophotal magnitudes. In the Appendix we give a derivation of the conversion between isophotal and total magnitudes as a function of magnitude or redshift. For distant galaxies there is up to a 0.8-mag correction owing to light lost.

Shape information is obtained from the higher central moments:

$$M_{ij} = \sum_A (x - \bar{x})^i (y - \bar{y})^j [I(x,y) - I_s], \quad i + j = 2, 3, \ldots . \quad (5)$$

Three of the seven shape discrimination features are the size, rotation, and translation invariant quantities computed from the central moments:

$$C_2 = (M_{20} + M_{02})/M_{00}, \quad (6)$$

$$C_4 = (M_{40} + 2M_{22} + M_{04})/M_{00}, \quad (7)$$

$$E = \frac{1}{M_{02} + M_{20}} [(M_{20} - M_{02})^2 + 4M_{11}^2]^{1/2}, \quad (8)$$

where C_2 and C_4 are the total second and fourth moments while E is a parameter that measures the elongation of the object. While it is true that C_2 and C_4 are strongly correlated, empirically it is found that there is sufficient additional information in the fourth moment to justify its use as an additional shape discrimination feature. The quantities in the above equations, including the sky intensity I_s, are computed in a single pass over the data and simple transformations are used to translate them into the canonical forms given. This added complexity is a concession to performance, since the entire object area cannot be held in fast memory for many larger objects.

In a second, partial pass over the same image data three additional quantities are determined: the peak intensity I_p is the difference between the local sky intensity and the average intensity evaluated in a 3×3 area centered on the object centroid. This is the fourth shape discrimination feature. The convolution S of the

object image and an ideal star image at the centroid is the fifth feature. The particular convolution used is the normalized nonlinearly scaled template matching operator (Rosenfeld and Kak 1976)

$$S = \left(\sum_A s(x-\bar{x},y-\bar{y})[I(x,y)-I_s]\right) \times \left(\sum_A [I(x,y)-I_s]^2\right)^{-1/2} \times \left(\sum_A s^2(x-\bar{x},y-\bar{y})\right)^{-1/2}. \quad (9)$$

The function $s(x,y)$ is an idealized star image obtained from averaging bright, unsaturated stars from a plate with good seeing. The quantity S has the value 1.0 for a perfect match between the template and the image. Note that in Eq. (9) the summation is over the area of the template image, not the image being evaluated.

The effective radius R_{ef} is the sixth shape description feature and is defined similarly to a moment:

$$R_{ef} = \frac{1}{M_{00}} \sum_A r[I(x,y)-I_s], \quad (10)$$

where r is the Euclidean distance from the point (x,y) to the object centroid. The seventh of the parameters used in the shape analysis or classification procedure is the object magnitude J.

During the object parameter evaluation process several consistency checks are made to ensure the object is a valid image of a star or galaxy. These tests do not eliminate all noise effects, but the volume of data to be scanned by the classifier is reduced. One set of tests requires that $M_{ij} > 0$ for all i and j evaluated. The second major check requires that $J \leq J_{lim}$, where J_{lim} is usually taken to be 24.5 mag. This limit was chosen to prevent an excessive number of dim objects or object-like artifacts from the plate from being included in the output list. If the consistency checks are satisfied and the object is brighter than the J_{lim}, a sequentially assigned name, flags indicating special conditions, and the various numeric parameters are added to the output list. In addition to the object list, separate files are maintained that contain the actual segmentation area definition and the full-resolution rectangular image areas used in the computations. These additional files allow reviewing the segmentation and classification processes by directly observing objects as well as redetermination of the object parameters without rerunning the segmentation process.

At the very low segmentation thresholds used, it is a common occurrence for the luminosities from two presumably physically distinct objects to overlap, e.g., a 20th-mag galaxy and a 17th-mag star closer than 10 arcsec. The segmentation, area assembly, and parameter evaluation processes will treat these as a single object. In order that the final list of objects more closely agree with manually derived lists, a procedure has been developed to separate such closely spaced objects. To separate close objects, the principle axis, a line through the object centroid at an angle θ,

$$\tan 2\theta = \frac{2M_{11}}{M_{20}-M_{02}}, \quad (11)$$

is scanned for multiple peaks. The strength of the peaks and the minimum spacing between them required before they will be recognized as distinct are computed from M_{00}. If two peaks are found along the principle axis, the area is assumed to contain two separate objects and it is divided into two areas by the normal to the principle axis located at the minimum intensity point found between the two peaks. Each area resulting from the splitting operation is reprocessed and again tested for multiple objects. A limit is established on how many times (usually 4) this iteration may proceed for an original area. Typically, areas containing two objects can be successfully separated if the magnitude difference between the two objects is less than 5 mag. In many cases, three closely spaced objects have been correctly separated, the maximum allowed by an iteration count of 4. Figure 2 shows the sequence of steps in separating a group of the closely spaced objects.

When this splitting procedure was first used, brighter spiral galaxies with well defined arms would occasionally trigger the splitting mechanism. To alleviate this problem, an additional test that the ratio of the sums of the absolute values of intensity changes along the principle axis to a similar sum computed along the normal to the principle axis intersecting at the minimum between the two peaks be greater than a threshold, was added. It has been determined that a value of 3 for this threshold prevents mutilation of brighter spiral galaxies without significantly affecting the desired separation of pairs or triples of object images.

Summarizing, the processes described in this section generate a list of object descriptions from the original digital plate image. Each object in the output list consists of a record with the following information: name; position relative to the plate origin; area in pixels; magnitude; the central moments M_{20}, M_{11}, and M_{02}; the total fourth moment; peak intensity; star image correlation; effective radius; local sky intensity; and flags indicating various exceptional conditions. Flags are used to indicate multiple objects in an area, the intersection of the object with the digitized region boundary or violation of maximum image size limitations. These data form the basic catalog with the first analysis performed being the classification.

IV. OBJECT CLASSIFICATION

The classification problem, distinction of resolved from unresolved images, is fundamentally one of shape discrimination, since color information is not available for all 12 fields at this time. Stellar images which are unresolved must be separated from galaxy images which have an extremely wide variation of size and shape for

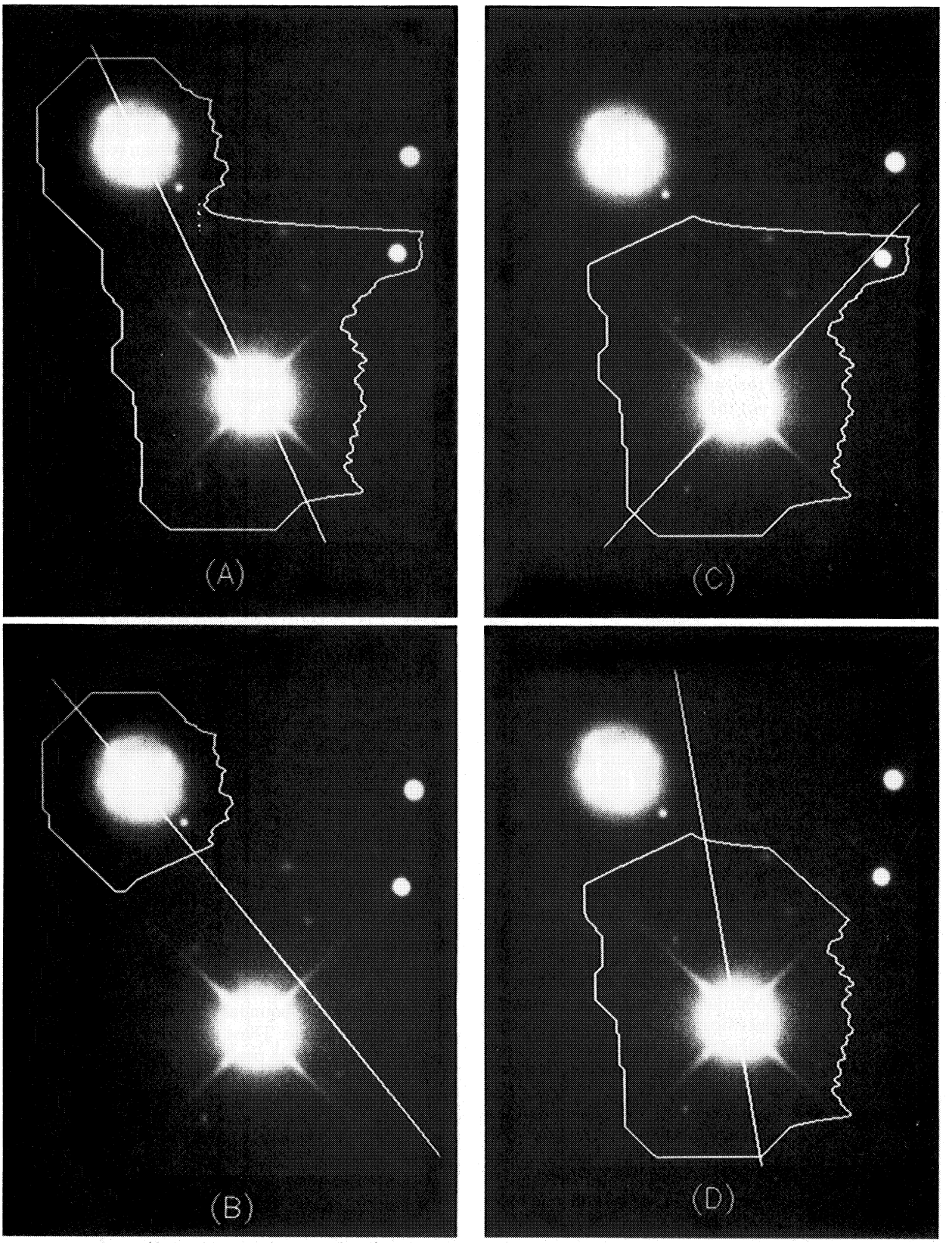

FIG. 2. A sequence of images showing the processing of a group of three objects originally segmented as a single area. The fourth object, in the upper right, was originally segmented as a separate object. The detection isophotes and principle axis are drawn on each image. In Figs. 2(a) and 2(c), two objects have been detected.

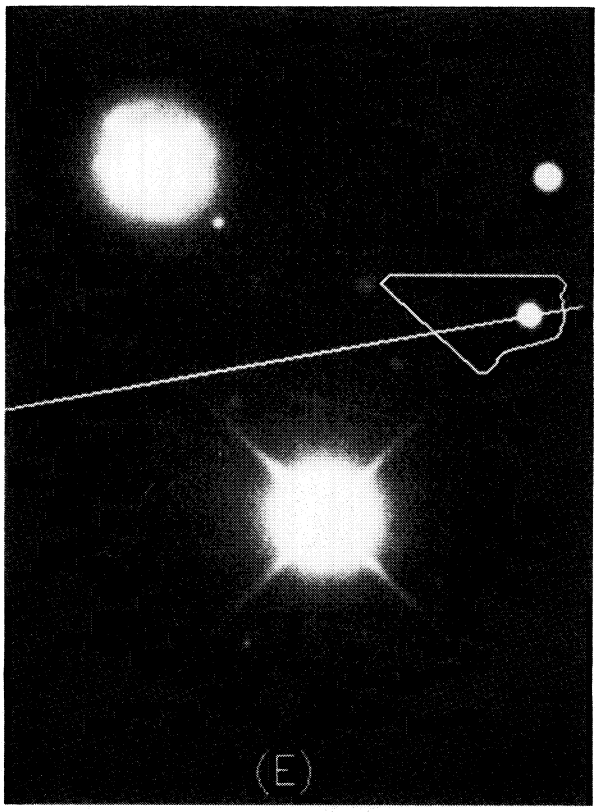

FIG. 2. (continued)

a particular magnitude. Stellar images have a finite size on the plate, but this is due to scattering in the atmosphere, telescope aberrations, and scattering in the plate emulsion. Of these, atmospheric scattering, "seeing," is the dominant effect for unsaturated images. Thus the details of stellar images are primarily a function of their apparent magnitude. For the brightest stars, diffraction spikes caused by the prime-focus cage support are also visible. As galaxies grow dimmer and more distant, they become progressively less resolved and appear to the eye almost indistinguishable from stellar images at the dim-object magnitude limit. In addition, most QSO's, faint BL Lacertae objects, and Seyfert galaxies are objects that have little or no obvious nebulosity and thus are stellar-like in appearance. Because of these effects a decision must often be made about the type of object when there is no clear-cut distinction. In practice, there is a continuum of objects ranging from clearly stellar to obviously galactic. Besides the primary classification problem, stars and galaxies, a variety of noise images are also found on the plates. These include lint, dust, pinholes, and occasional tape errors. The classifier must also identify these objects so they may be eliminated from subsequent analysis.

The basic approach adopted is a nonparametric statistical classifier (Batchelor 1974). In this approach, each object is characterized by a vector in a space defined by the set of measurements computed for each object image. The classification problem is then the design of a surface in this space that separates, with minimum errors, the volume containing star vectors from the volume containing galaxy vectors. We will describe a two-stage procedure for arriving at specific surface design for each plate and the considerations that led to the particular surface form used.

A possible alternative would be the Baysean or parametric classifier as described in Sebok (1979). While this method is attractive because it is optimal under the assumptions made in its design, it appears to be more sensitive to noise at the dim limit than the nonparametric classifier and does not fully utilize all the information that is available about each object image. Moreover, some of the data required in its design are the object of the observational program that led to the need for the classifier. A comparison of the Sebok classifier and the nonparametric method to be described will be given in Sec. VI.

The shape characterizing parameters form a vector **F** locating each object in a seven-dimensional space:

$$\mathbf{F} = (J, C_2, C_4, E, I_p, S, R_{\rm ef}). \qquad (12)$$

The number of dimensions used in the classifier is a function of the data to be classified, not an intrinsic quantity in the classifier. The classification problem is finding a hypersurface in this space that separates the vectors of the three classes (noise, stars, galaxies) with maximum accuracy. In the first design step, the 7-space is divided into three regions by an operator at the interactive graphics station. Noise and star regions are approximated by separate areas in two different magnitude ranges on two scatter plots. Note that each scatter plot represents a different projection of the 7-space onto two dimensions, thus the areas on the scatter plots correspond to volumes in the 7D classification space. In these scatter plots, stellar images form a well defined boundary to the area occupied by points from stellar and galactic images. Noise image points occupy regions of these planes corresponding to smaller and sharper images than stars. This is in agreement with visual examination of many objects classified as noise. This manual division of the scatter plots into three regions is also consistent with the notion that unresolved objects (stars) show the combined atmosphere-optics-emulsion point spread function and therefore are the smallest possible images of astronomical objects at a given magnitude. For bright objects ($J < 19$) the effective radius $R_{\rm ef}(J)$ projection provides excellent discrimination. Figure 3 shows a scatter plot of the $R_{\rm ef}(J)$ data from one plate and includes the segmentation curves that were manually drawn. For dim objects ($J > 18$) the peak intensity $I_p(J)$ scatter plot allows an adequate initial separation. Figure 4 shows such data and the hand-drawn segmentation curves in this magnitude region. Hand-drawn curves are prepared individually for each plate, since there is too much variation in these parameters to allow common decision curves for several plates. This set of decision surfaces,

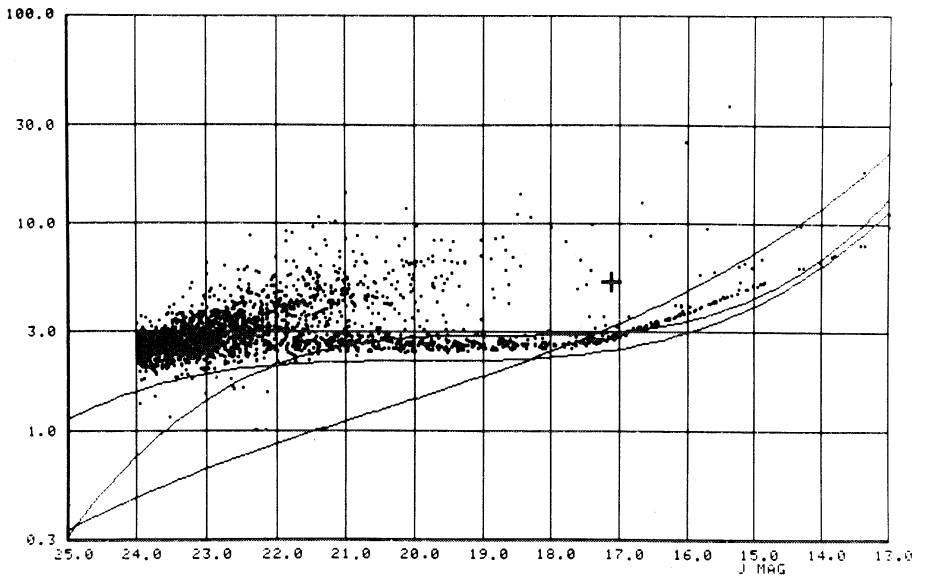

FIG. 3. The total effective radius vs magnitude, $R_{ef}(J)$, scatter plot for approximately 1000 objects from KP2345. The continuous curves are the manually drawn segmentations discussed in the text.

which are designed to overlap in the $19 \leq J \leq 18$ mag range, give adequate results for noise discrimination but do not fully employ all the information available and thus cannot do an optimal classification of stars and galaxies.

In a properly scaled scatter plot where number contours are plotted, the stellar branch is visible to much fainter magnitudes. Figure 5 shows such an isonumber density contours of the scatter plot in Fig. 4 linearly scaled and smoothed to enhance the contrast between the stellar and galactic regions of the data. A "valley" separating the galaxy region (broad peak in lower region) from stars (well defined ridge in upper area of plot) can be tracted to approximately 23rd mag.

Final classification is accomplished by an automatic procedure for defining a volume in the 7-space that encloses star vectors. This procedure requires a set of points (training set) in the classification space that has known classifications. Since no *a priori* classification information is available, a clustering technique which groups points that are close in the 7-space must be employed to generate the labeled training set. The initial, manually designed, classification is used to assign the labels of the clusters. The implicit assumption in this is that similarly shaped object images occupy compact regions of the 7-space and that the manual classification is a fair approximation to the final classification. The details of the automatic classifier follow.

First, a randomly chosen subset consisting of approximately 800 objects in the brightness range $19 \leq J$

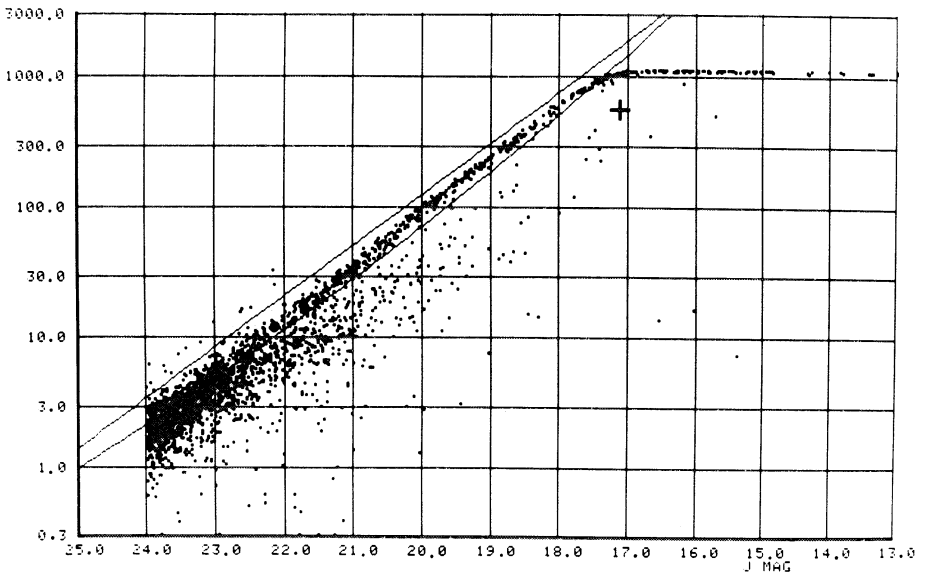

FIG. 4. The peak intensity vs magnitude, $I_p(J)$, scatter plot and segmentation curves for the objects displayed in Fig. 3.

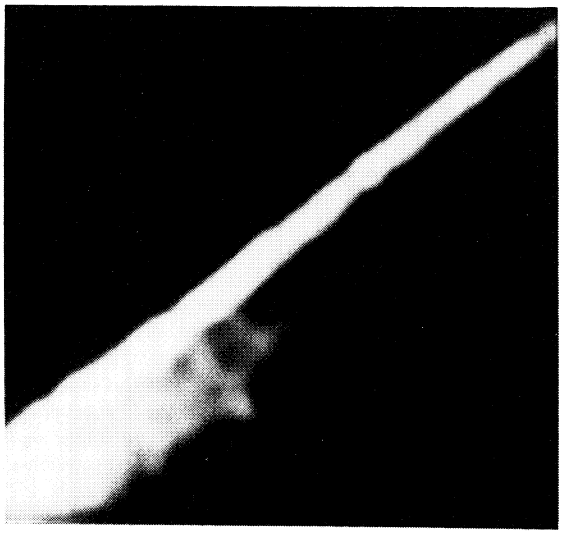

FIG. 5. Number density contours of the data displayed in the 19 to 24 mag range in Fig. 4. The number density has been linearly scaled and smoothed to enhance the different regions of the scatter plot. Note that the stellar region is observable to a significantly dimmer magnitude than in Fig. 4.

≤ 24 is taken from the complete object list. In order to compensate for the very rapid increase in the number of objects at faint magntiudes, bright objects are given a higher probability of being included in the subset. Next, either the individual parameters or their natural logarithms are normalized to the range 0 to 1. The logarithm is used for rapidly varying features such as the moments or peak intensity. Using the star-labeled points, quadratic scaling functions are determined for the six normalized parameters as a function of the seventh, J. Scaling also helps compensate for the great variation in relative number of the two classes as the object brightness varies between $J = 24$ and $J = 19$. Each of the objects in the subset is classified by the manual classification surfaces previously described. This normalized, scaled, and classified subset is partitioned into a number (typically 10) of compact clusters by a variant of the ISODATA algorithm (Ball and Hall 1967). The distance measure used to determine cluster membership is the Euclidean distance from the object vector to the cluster center in the 7D classification space. After all vectors are assigned to clusters, each cluster is given a label (star, galaxy, or ambiguous) depending on the fraction of vectors originally labeled star that are in the cluster. If the fraction of vectors classified as stars in the training set is η, a cluster is labeled star if its fraction of stars is $\geq 1.2\eta$. Similarly, if the fraction of star vectors in a cluster is $\leq 0.8\eta$ the cluster is given the galaxy label. Clusters containing star fractions near η are given the ambiguous label. If ambiguous clusters are present, the number of allowed clusters is increased and the clustering process is repeated. When a subdivision of the training set into a set of clusters with no ambiguous labels is achieved, the decision surface design routine is executed.

The decision surface is one or more hyperellipsoids, each enclosing some star vectors. The choice of hyperellipsoids instead of simpler surfaces was made after evaluating classifiers using a variety of surfaces. Each star-labeled cluster is used as the center of a hyperellipsoid that is hypothesized to contain star vectors:

$$S_i = 1.0 - \sum_{j=1}^{7} \frac{(f_{ij} - \bar{c}_j)^2}{a_j}, \tag{13}$$

where f_{ij} is the jth component of the ith object feature vector, [Eq. (12)], $\bar{c}_j$ is the cluster center for the jth component, and a_j is the square of the width of the hyperellipsoid in the jth coordinate. If $S_i > 0$ then the point F_i is inside the decision region and is classified as a star. The training set where each object is classified according to the cluster it was assigned to is used iteratively to adjust the 14 parameters, $\bar{c}_j$ and a_j, to achieve a minimum classification error. The procedure is similar to the compound classifier training rules (Batchelor 1974). In particular, if the training label is star and F_i does not fall within one of the hyperellipsoids, the closest hyperellipsoid to F_i is enlarged in the direction needed to enclose the point. If the training label is galaxy, each hyperellipsoid containing the misclassified point is shrunk as needed to exclude the point. For either type of error correction the training rules are

$$\begin{aligned} \bar{c}_j^{k+1} &= \bar{c}_j^k + \Delta_p(f_{ij} - \bar{c}_j^k), \\ a_j^{k+1} &= a_j^k - \Delta_s(f_{ij} - \bar{c}_j^k)^2 \end{aligned} \tag{14}$$

for all components j of each hyperellipsoid to be modified. The superscript k counts the iterations made with the training set. The signs of the correction terms correspond to misclassified stars. If the correction corresponds to a misclassified galaxy the signs of the correction terms are reversed. The quantities Δ_p and Δ_s control the rate of convergence of the procedure. Hyperellipsoids are allowed to disappear if they become sufficiently small that they contain no star-labeled vectors. However, hyperellipsoids are not formed during the training process. After a fixed number of iterations through the training set, parameters are obtained that result in a small and stable number of misclassifications. In many cases, only one of the originally hypothesized hyperellipsoids remains. The quadratic scaling polynomials and the hyperellipsoid parameters generated during the training are used to classify all the objects, including the training set, that have $J \geq 20$ mag.

This classifier, while empirical, appears to work very well. In particular, when used recursively, the number of objects of a particular kind remains stable. That is, given a prior classification, either the initial manual or a subsequent automatic, the relative proportions of the two classes do not change significantly, if another iteration of the automatic classifier is made. Simpler decision surfaces, hyperspheres or hyperplanes, did not show this property. In addition, this classifier does not require that the features used be linearly independent or that they be drawn from a homogeneous set of parameters.

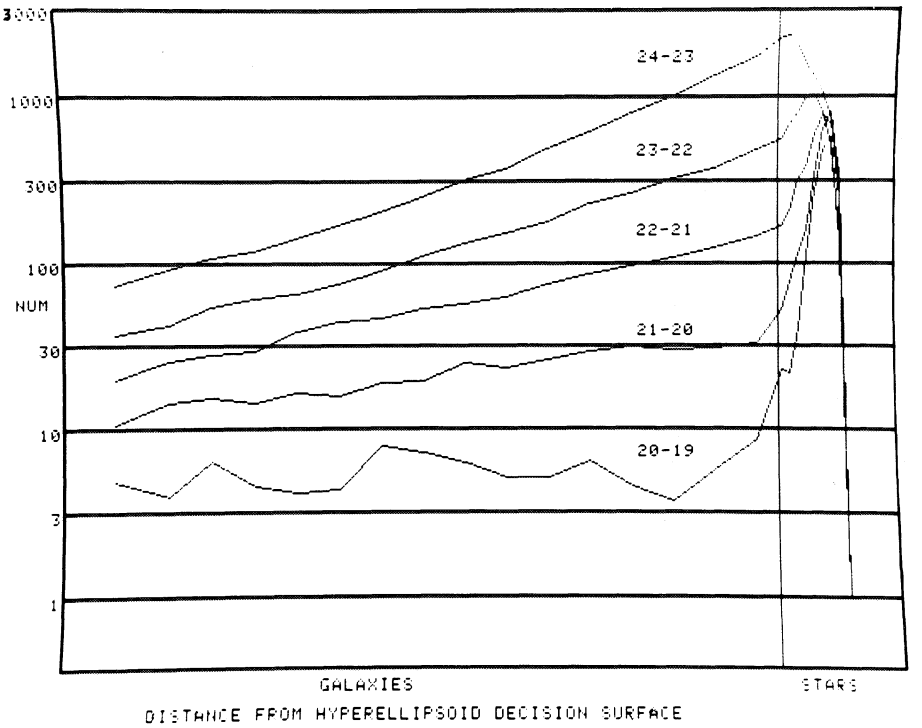

FIG. 6. The histogram of the number of objects found at the indicated distance (arbitrary units) from the classification surface. This plot shows a summary over the 12 plates processed by FOCAS. In future we will make a statistical correction for misclassified galaxies.

One way of displaying the results of the classification is to plot a histogram of the number of objects found at a given distance from the decision surface (Fig. 6). Note the strong peaks to the right of (within the hyperellipsoid) the decision surface. A dominant peak is expected here because stellar images are expected to be quite homogeneous. To the left of the decision surface is the galaxy region. For the two brighter summary curves ($20 \leq J \leq 22$) clearly defined but very broad peaks can be seen in the galaxy region. For the dimmer summary curves there is the expected continuum of objects between the stellar-like and clearly galactic-like images. Moving the decision surface by 10% of the distance to the star peak changes the classification of about 2.5% of the objects in each magnitude range. This interpretation of a well defined region of star vectors is substantiated by investigations made with a nonlinear cluster displaying procedure (Sammon 1969).

The $J = 20$ bright limit used for the automatic procedure is required because the central regions of star images begin to saturate near this value and there is a noticeable change in the variation of star features with magnitude at about this magnitude. Objects brighter than 20th mag continue to be classified reliably by the manually designed relationship in the $R_{ef}(J)$ subspace. As it is, some broadening of the $19 \leq J \leq 20$ star curve can be seen in Fig. 6.

The final step in the preparation of the classified set of objects is to review the classification of all objects brighter than 20th mag. The program used allows for reclassification and provides a capability to change or redo the results of the multiple object splitting procedure.

An attempt was made to correct several of the computed image parameters for the effects of the 4-m prime-focus camera pincushion distortion (Chiu 1976), with the intent of reducing scatter and thus allowing a more precise classification. This procedure did not seem to help and was not used in the production of the final catalog.

The final step in the preparation of a catalog file from a plate is to make a correction to the magnitude of stars with saturated cores. Based on the magnitudes of a number of brighter stars found on the 12 plates, a quadratic correction, relating the FOCAS calculated magnitude to those given for the brighter stars, was generated. The quadratic was manipulated so its roots were approximately equal to the magnitude where the $I_p(J)$ scatter plot shows the onset of saturation in stars. The resulting correction was then applied to all star images brighter than the value of the lower root ($J = 17.54$). While it is an oversimplification to use the same correction on all plates, it is a sufficiently good approximation that star counts are more limited in accuracy by $\sqrt{N}$ counting statistics than photometry at 13th mag.

V. CATALOG MAINTENANCE

The preceding sections have described the method for taking raw plate images and reducing them to a list of

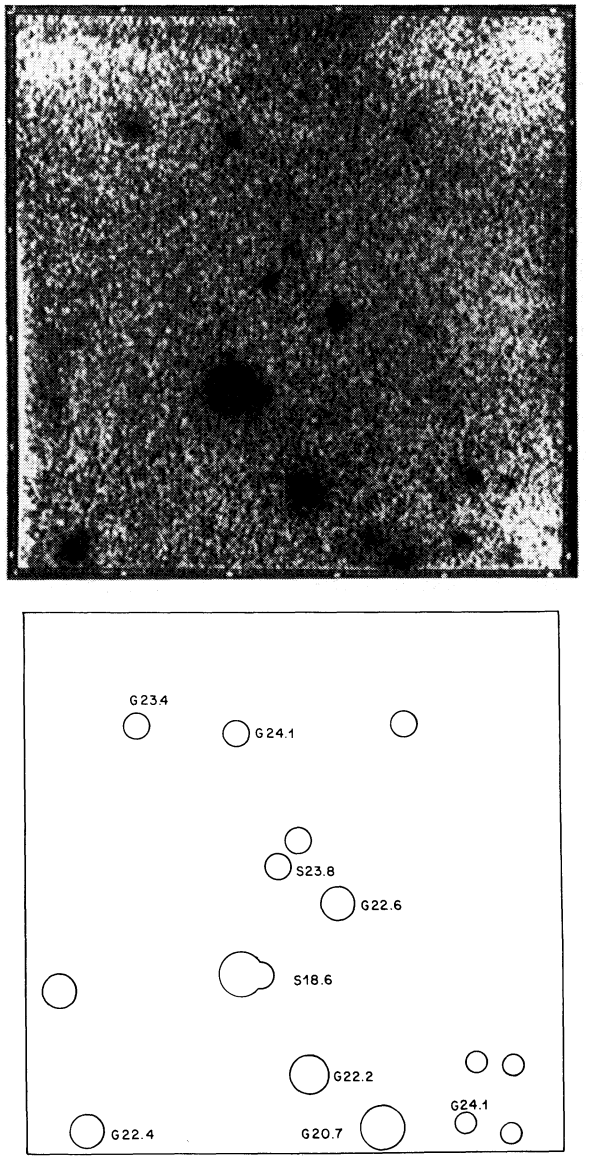

FIG. 7. (top) A 40-min exposure with the 4-m video camera of the 3C 268.2 field which goes deeper than a limit plate. (bottom) Objects visually identified in the field. The magnitude and type classification are given if the object was detected by FOCAS on plate KP2742.

objects of known apparent magnitude and type. A catalog in FOCAS is a collection of object lists, one for each plate, that have been subjected to some selection criteria. For example, a catalog could be all the galaxies dimmer than 21st mag. The power of the FOCAS system for analysis of such catalogs stems from the ease that selected subsets of objects may be prepared. Four specific design criteria are used to allow this ease of catalog manipulation.

The first of these is the design of the file format for the object lists. There is normally one master file associated with each plate in the catalog. Each object list (or file) consists of a header record containing certain plate specific data (plate name, field name, galactic coordinates, segmentation run date, processing parameters) and one entry for each object in the list. The object record includes the specific quantities given in Sec. III, the type assigned by the classifier, and the computer-assigned name.

Second, where appropriate, the various classification and analysis programs accept as input and produce as output the standard file format. This very simple concept allows iterative or repetitive applications of the basic programs to obtain the desired data from a plate master file.

Third, where possible, object data are kept in a form that is independent of the specific plate characteristics. In particular, apparent magnitude, a type classification field, and a common plate scale factor allow comparison and summary of data over several plates. This is not true of the basic shape discrimination features, which are quite dependent on the specific processing and exposure conditions used to prepare the plate, particularly the seeing conditions.

Fourth, the UNIX timesharing system command line processor, "shell," is used to implement a catalog processing language. Given the first three design rules, the command interpreter provides the facilities for applying sequences of programs to each object file in a catalog. Since sequences of commands (programs) including looping and branching operators can be stored in files and executed as though they were simple commands, powerful selection criteria may be programmed simply and naturally. These system-provided facilities greatly simplify the bookkeeping needed to specify and guarantee comprehensive searches of the complete catalog.

Programs that are available, some providing color interactive data displays, include object selection, number counts, parameter printing, parameter mean and standard deviation summaries, classification, list merging, analysis, and field comparison routines. The classification group includes both the manual and automatic classifiers as well as clustering display programs. Testing has been facilitated by programs that generate data of various kinds from models. These simulation tests will be discussed in detail in Sec. VI.

VI. FOCAS PERFORMANCE AND TESTING

At present, there is no existing catalog that can be used to provide an independent check of the results of FOCAS at its dim-object limit. In order to gain confidence in FOCAS, a variety of tests and simulations have been done to assess the reliability, accuracy, and completeness of the catalogs it produces.

The first test measures detection efficiency down to the $J = 24$ limiting magnitude. Two plates of comparable quality showing the same field were processed. In this comparison the lists of objects were 97% common down to 24th mag. By 24.5 mag, 75% of the objects in one list

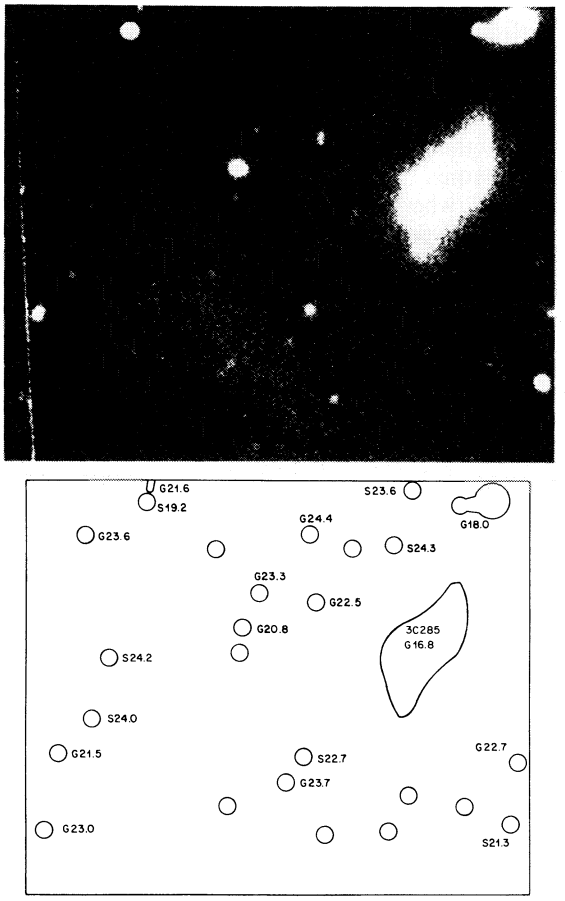

FIG. 8. (top) Photographic sum of four plates showing 3C 285. (bottom) Visual detection of the objects at top with the results of processing the appropriate area of KP2343 given as labels. The 21.5-mag object at the left (east) and the 21st-mag fuzzy QSO (center) are detected, correctly classified, and given correct magnitudes by FOCAS.

could still be found in the other. Lack of commonality in the two lists can be due to either noise contamination or poor detection efficiency. These two plates and a third one were summed on a pixel-by-pixel basis and the summed data were processed by FOCAS. The resulting list of objects appears to be more complete and to have a significantly lower noise contamination at dimmer magnitudes than any single plate of the same field. Spot examination of a few objects by either photoelectric photometry or CCD and video camera imagery on the 4-m also confirms the claims made about detection efficiency and the magnitude scale. An example is shown in Fig. 7(top), where a deeper exposure made using the video camera on the 4-m is labeled by the results of processing a plate (KP2742) including the same field with FOCAS. Figure 8(top) shows four photographically summed plates of the 3C 285 field (Saslaw *et al.* 1978) and the comparison with the same area on plate KP2343 processed by FOCAS. In Figs. 7(bottom) and 8(bottom), objects in the deeper images have been visually identified, and detection by FOCAS is indicated by listing the magnitude and classification next to the identified image. The fraction of faint objects detected by FOCAS appears consistent with the 24th-mag cutoff in the catalog, and there are no identifiable cases of object misclassification by FOCAS in these examples.

A second test was processing a uniformly fogged plate. This test was conceived as a means of assessing the contribution of small, very low surface brightness images that might come from emulsion irregularities. The fog density was comparable to the sky density in plates normally processed. Since no sensitometer data were available, a characteristic curve and zero point from a plate of the same batch with its sky density most comparable to the fogged plate were used for the test. In this test no significant number of objects were found brighter than $J = 24$. Some lint or dust was found brighter than this, a common occurrence, but the normal classification presumably would have identified these objects. The number of these nonastronomical images rises slowly ($\approx 10^{0.3J}$) with magnitude until $J \approx 24.5$ mag, where the grain noise contribution begins to rise sharply, limiting photographic detection brighter than this point.

In another test, an idealized star image was created by averaging images in the $20 \leq J \leq 22$ range from a low-latitude plate (KP2345) exhibiting very good seeing. This is the same image used in the template evaluation, Eq. (9). These data were also used to create simulated plate images each containing 192 stars with identical peak densities that were then processed by FOCAS. The emulsion characteristics were simulated by adding normal random noise with a standard deviation of 2.5 density units, which is typical of the plates processed. The variation in parameters of the simulated stars for each image would be expected to give information about the precision of the parameters computed by FOCAS in different magnitude ranges. Tables III–V list the results, both the average values and standard deviations, of this simulation and a similar set of parameters computed in 0.3-mag intervals for stars and galaxies from KP2345. There is good qualitative agreement between the simulated stars and the stellar data from the plate. From the "No." column for the simulations it can be seen that the detection efficiency is very high (the total number created in each group is 192). The average differences in the computed image parameters between stars and galaxies are also apparent in these tables.

A test of the classification method was made using entirely synthesized image data, both stars and galaxies. These data were processed and classified in the same way as actual plate material. Unlike objects derived from plates, the origin, and therefore the type, of each synthesized object is known, thus comparisons between the classifier results and image type can be made. This test is only a qualitative indication of the accuracy of the classifier, since the synthetic data do not completely model the actual images.

In this test a total of 840 star and 2937 galaxy images were created between 20th and 24th mag. The star-

TABLE III. Stars—simulation results.

No.		J	R_{ef}	C_2	C_4	I_p	S	E
189	Mean	23.90	2.24	6.3	7.75	2.47	0.6103	0.284
	σ	0.16	0.28	1.7	2.61	0.30	0.0425	0.152
186	Mean	23.55	2.29	6.6	8.16	3.22	0.7119	0.229
	σ	0.11	0.18	1.2	2.04	0.24	0.0302	0.110
191	Mean	23.35	2.22	6.3	7.98	4.08	0.7894	0.236
	σ	0.10	0.21	1.4	2.44	0.26	0.0262	0.121
189	Mean	22.94	2.26	6.5	8.24	5.90	0.8727	0.198
	σ	0.06	0.16	1.1	2.36	0.28	0.0158	0.095
191	Mean	22.54	2.33	7.1	9.35	8.30	0.9298	0.139
	σ	0.05	0.13	1.0	1.88	0.24	0.0079	0.073
192	Mean	22.16	2.33	7.1	9.26	11.69	0.9630	0.124
	σ	0.03	0.09	0.7	1.67	0.28	0.0045	0.060
192	Mean	21.76	2.43	7.9	11.13	16.52	0.9810	0.101
	σ	0.03	0.10	0.8	1.85	0.29	0.0017	0.052

TABLE V. Galaxies—plate KP2345.

No.		J	R_{ef}	C_2	C_4	I_p	S	E
1204	Mean	23.85	2.57	7.7	8.56	1.91	0.3366	0.386
	σ	0.09	0.27	1.8	2.32	0.57	0.0501	0.208
957	Mean	23.56	2.70	8.7	9.99	2.34	0.3971	0.332
	σ	0.09	0.30	2.1	2.74	0.67	0.0614	0.197
685	Mean	23.26	2.89	10.2	12.13	2.92	0.4650	0.361
	σ	0.09	0.41	3.5	4.22	0.88	0.0810	0.197
515	Mean	22.96	3.11	12.0	14.54	3.55	0.5277	0.361
	σ	0.09	0.48	4.1	5.13	1.11	0.0916	0.187
411	Mean	22.64	3.33	14.0	17.34	4.46	0.5933	0.353
	σ	0.09	0.52	4.7	5.87	1.38	0.0976	0.187
311	Mean	22.35	3.54	16.0	20.15	5.47	0.6535	0.339
	σ	0.09	0.63	6.2	8.21	1.71	0.1136	0.178
258	Mean	22.06	3.77	18.9	24.52	6.79	0.7017	0.337
	σ	0.09	0.83	11.1	19.91	2.49	0.1224	0.178

image synthesis method is as described previously, except that peak intensities were chosen from an exponential distribution to obtain approximately equal numbers of stars per magnitude range. Galaxy images were created in approximately equal numbers from both inverse r^2 (elliptical) and exponential (spiral) light distributions (Holmberg 1975). For each type the core radius, central surface brightness, and ellipticity were varied in an attempt to match the observed number versus magnitude trends as well as other parameter distributions. The resulting images were convolved with the stellar image to simulate seeing, and finally a normally distributed noise was added to each pixel. Brighter than 23rd mag the overall correct classification was 97.8%, 98% for galaxies, and 97.3% for stars. In the 24th and 23rd mag range, the overall correct classification was 87%, with 89% of the galaxy images and 73% of the star images correctly classified. Again, while this is only a qualitative indicator of the classifier performance, we feel it is indicative of the classifier performance when applied to actual data. Thus in a homogeneous sample of stars and galaxies to 24th mag, we expect at least 90% of the galaxies and 80% of the stars to be correctly classified.

TABLE IV. Stars—plate KP2345.

No.		J	R_{ef}	C_2	C_4	I_p	S	E
122	Mean	23.85	2.13	5.5	6.13	2.94	0.4279	0.458
	σ	0.08	0.12	0.7	1.51	0.40	0.0313	0.208
197	Mean	23.55	2.19	5.9	6.89	3.70	0.5151	0.376
	σ	0.09	0.13	0.8	1.28	0.51	0.0421	0.185
212	Mean	23.25	2.29	6.5	7.79	4.62	0.5967	0.275
	σ	0.09	0.15	0.9	1.49	0.66	0.0406	0.143
217	Mean	22.97	2.38	7.1	8.73	5.74	0.6771	0.274
	σ	0.09	0.16	1.0	1.45	0.78	0.0406	0.139
183	Mean	22.65	2.46	7.6	9.67	7.53	0.7593	0.256
	σ	0.09	0.17	1.1	1.14	1.73	0.0400	0.120
165	Mean	22.35	2.50	8.0	10.56	9.92	0.8280	0.231
	σ	0.09	0.19	1.3	2.03	1.49	0.0352	0.122
150	Mean	22.06	2.54	8.4	11.31	12.87	0.8775	0.223
	σ	0.09	0.19	1.3	2.05	1.84	0.0284	0.106

The catalog of synthesized star and galaxy images was also classified by the parametric or Baysean classifier given by Sebok (1979) [Eq. (15)]. For the classification test a Hubble-law luminosity distribution with a core radius of 0.74 arcsec was used. The resulting distribution was convolved with the stellar image prototype to model more closely the actual galaxy images. A value of the decision parameter, $\phi = 0.84$, was chosen as the minimum value that would correctly classify stars brighter than 22.5th mag. Using this classifier, we find that greater than 99% of both star and galaxy images brighter than 23rd mag are correctly classified. In the 24th and 23rd mag range, star classification accuracy was 90% and the galaxy classification accuracy was 80%. In the dim range the elliptical model was classified somewhat better than the spiral model galaxies. Presumably, the slower decrease in luminosity of the inverse r^2 distribution relative to the exponential distribution was responsible for this difference. Note also that the galaxy classification accuracy drops more rapidly than the star classification accuracy, which is the opposite behavior of the nonparametric classifier used in FOCAS. In addition, it is likely that a decision parameter in the form $\phi(J)$ can be designed that would yield a better overall classification than was achieved in these simulations.

We have obtained, courtesy of R. Kron, his results of processing the SA 57 field (Kron 1980), plates KP1561 and KP1562. This allowed an object-by-object comparison with the results obtained by processing KP1561 with FOCAS. For inclusion in Kron's catalog an object must be found on each of a pair of plates in either one of two color bands (J and F). This process ensures that his results are not significantly contaminated by noise. To match objects from the two catalogs, the coordinates of objects in Kron's catalog were transformed to the

TABLE VI. Kron—FOCAS processing comparison.

Magnitude range	N	% match	Δm	% same
24.0–23.5	4635	65.1	0.18	81.1
23.5–23.0	2656	88.2	0.21	85.6
23.0–22.5	1262	91.7	0.09	88.5
22.5–22.0	724	89.4	0.00	90.7
22.0–21.5	425	88.5	−0.09	91.7
21.5–21.0	298	92.6	−0.16	92.4
21.0–20.5	193	94.8	−0.20	92.3
20.5–20.0	102	99.0	−0.22	85.1

FOCAS coordinate system and subsets of objects in 0.5-mag intervals within the plate area processed by FOCAS were prepared. Each of the subsets was matched with the total FOCAS catalog for plate KP1561. Those objects in the Kron subset that were within 3.5″ of an object in the FOCAS catalog were considered matched. The mean matching distance was 1.4″. Since the catalog is magnitude limited at $J = 24.5$, it is likely that a large fraction of the mismatches in the fainter magnitude bands are due to this, in combination with a matching standard deviation of 0.3 mag. Since the Kron catalog includes objects found in the F-band but not detectable in the J-band plates, it will be more complete for dim red objects than the FOCAS catalog. This is another factor leading to mismatches in the faint magnitude bands. Examination of the average properties of the matched and unmatched lists of objects in the Kron catalog indicates the unmatched objects have a larger effective radius and a smaller peak density than the matched objects. This is consistent with the FOCAS detection limits that were set to exclude most objects that would appear to be primarily from emulsion irregularities. The results of the matching, which are considered excellent given the very different techniques used in the construction of the two catalogs, are summarized in Table VI. In Table VI, N is the number of objects from the Kron catalog in the magnitude range, % match is the percentage of the N objects found in the FOCAS catalog, $\Delta m = J_{\mathrm{FOCAS}} - J_{\mathrm{KRON}}$, and % same is the percentage of the matched objects having the same classification in the two catalogs.

A typical plate is analyzed to a list of 7200 objects brighter than 24th mag in a 12-hr processing run. A total of 1.2×10^7 bytes are stored in the 11/45 file system during this step. This represents about a 3:1 total data reduction from the original data, with the majority of the stored data being the individual full-resolution object images. Classification requires approximately $\frac{1}{2}$ hour at the interactive display and about an equal time spent executing the automatic classifier.

VII. RESULTS

The dynamic range, the range of actual object magnitudes that can be processed by FOCAS, extends from a dim limit of 24th mag to approximately 13th mag for galaxies and to 6th mag for stars. The dim limit is determined from the system noise, primarily the emulsion, while the bright limits are due to size limits on objects imposed by the FOCAS software. These limits hold for IIIa-J plates exposed on the KPNO Mayall 4-m telescope that have sufficient exposure to bring the sky density above the toe in the characteristic curve, a prerequisite for inclusion of plates in our catalog. Since the magnitude computations are done after the conversion of density values into intensities, the effective calibrated range of FOCAS extends from 24th mag to bright limits determined by the onset of emulsion saturation. For galaxies, saturation typically occurs for total apparent magnitudes of 13 to 14, while for stars saturation occurs in the 17th to 18th mag range. Within this region, the magnitudes are defined to within a constant by the characteristic curve calibration, thus apparent magnitudes for all objects may be calculated knowing the magnitude of a single (unsaturated) object on the plate. When magnitudes for more than one object are available, a measure of the linearity and repeatability of the FOCAS magnitude scale can be obtained. In particular, two of the plates processed were exposed in Selected Areas 57 (KP1561) and 68 (KP1286) and include B and V photoelectric stellar sequences down to $B = 22.5$ mag. Using the transformation $J = B - 0.23(B - V)$ (Kron 1980), we computed J magnitudes for the sequences. Comparing the FOCAS J magnitudes to these standard sequences yields $\sigma = 0.087$ mag for 15 stars with $22.21 \leq J \leq 18.16$ in KP1561 and $\sigma = 0.065$ mag for 21 stars with $21.99 \leq J \leq 18.08$ in KP1286. Any systematic differences between the standard sequences and the FOCAS magnitudes are less than the standard deviations given.

While stellar images saturate in the 17th to 18th mag range, the magnitude given by FOCAS brightward of the saturation point is a monotonic increasing function of the actual magnitude. Sequences of stellar magnitudes

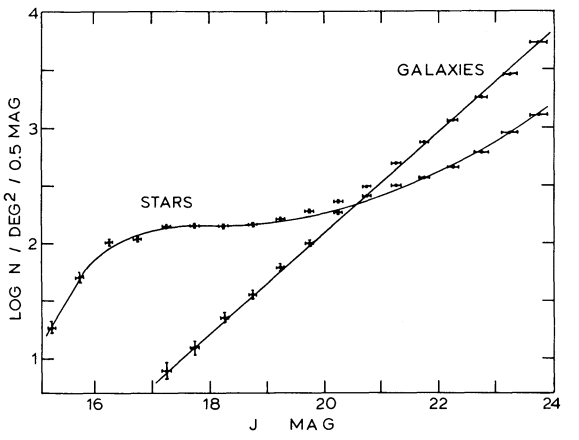

FIG. 9. Differential galaxy and star counts per magnitude per square degree. Our observed cumulative galaxy number counts for $J > 17$ mag follow the relation $\log N = 0.443J - 6.45$. Significantly, there is no evidence for a bump at the faint end, implying little apparent galaxy evolution to 24th mag, therefore large galaxy-formation redshifts.

TABLE VII(a). Differential galaxy counts.

Plate J magnitude	1286	1561	2334	2343	2345	2739
13.5–13.0	0	0	0	0	0	0
14.0–13.5	0	0	0	0	0	0
14.5–14.0	0	0	1	1	0	0
15.0–14.5	0	0	0	0	0	0
15.5–15.0	0	1	1	1	0	0
16.0–15.5	0	0	0	1	3	1
16.5–16.0	0	0	2	2	2	0
17.0–16.5	0	2	1	4	3	0
17.5–17.0	1	2	2	8	6	1
18.0–17.5	6	3	6	13	8	2
18.5–18.0	8	10	3	16	13	3
19.0–18.5	6	16	17	17	28	9
19.5–19.0	19	17	19	39	36	16
20.0–19.5	25	23	43	66	66	22
20.5–20.0	48	81	66	109	108	41
21.0–20.5	86	149	114	170	177	83
21.5–21.0	165	217	154	245	267	137
22.0–21.5	260	319	267	378	342	196
22.5–22.0	385	582	392	482	468	333
23.0–22.5	655	875	590	760	710	494
23.5–23.0	1031	1403	958	1154	1148	832
24.0–23.5	2556	2385	2187	2375	1820	1586

TABLE VII(b). Differential galaxy counts.

Plate J magnitude	2740	2741	2742	2743	2747	2766	12 plates
13.5–13.0	0	1	0	0	0	0	1
14.0–13.5	0	0	0	0	0	0	0
14.5–14.0	0	0	0	0	1	0	3
15.0–14.5	1	0	0	0	0	0	1
15.5–15.0	0	0	1	0	1	0	5
16.0–15.5	0	0	0	0	2	0	7
16.5–16.0	0	2	1	0	0	0	9
17.0–16.5	1	0	0	1	4	0	16
17.5–17.0	1	3	1	4	4	2	35
18.0–17.5	2	5	2	2	5	1	55
18.5–18.0	8	13	10	6	6	7	103
19.0–18.5	5	13	11	18	12	8	160
19.5–19.0	20	26	27	27	12	20	278
20.0–19.5	22	52	46	25	34	26	450
20.5–20.0	66	70	73	64	53	59	838
21.0–20.5	102	109	134	120	78	72	1394
21.5–21.0	152	169	223	191	135	125	2180
22.0–21.5	274	285	353	295	284	175	3428
22.5–22.0	375	468	545	454	483	317	5284
23.0–22.5	659	763	864	707	738	436	8251
23.5–23.0	994	1144	1251	1131	1080	726	12852
24.0–23.5	1479	1928	2671	2605	1824	1235	24651

in the saturation region allow the construction of a correction relationship to convert FOCAS magnitudes to apparent magnitudes. An average correction of this kind was determined and applied to the stellar data given in Table VIII. At a stellar magnitude of 13, FOCAS typically indicates 15th mag with a slope of 0.5 FOCAS mag per actual magnitude change.

The resulting differential number counts for the magnitude-limited sample, classified as stellar and galactic, are shown in Fig. 9. A tabulation of these data is given in Tables VII and VIII. Our selection function begins to drop significantly at $J = 24.5$ mag, so that the data to 24th mag need no selection correction. Magnitudes are isophotal (to 26.5 mag/arcsecond^2) and are uncorrected except for atmospheric extinction and bright-star saturation. In the Appendix we derive corrections for zero-redshift isophotal magnitudes. The number of galaxies versus galactic latitude at constant magnitude J fits the secant extinction law with a coefficient of 0.3 mag. The cumulative number of galaxies found at high latitude (nine fields, $b^{II} \geq 45°$) is 14300 $\pm$ 640 per square degree at $J = 24$ mag. The dispersion in this number between single high-latitude fields, after correcting for differential galactic extinction, is 2300 per square degree. This is larger than the $\sqrt{N}$ error of 120 owing to inhomogeneities from galaxy clustering and high-latitude clumped extinction. The differences between these values and the 17100 per square degree re-

TABLE VIII(a). Differential star counts.

Plate J magnitude	1286	1561	2334	2343	2345	2739
<13.00	2	3	6	4	12	3
13.5–13.0	2	0	5	3	4	4
14.0–13.5	2	1	9	6	16	5
14.5–14.0	3	6	9	3	14	7
15.0–14.5	3	7	14	6	36	11
15.5–15.0	7	10	15	8	48	14
16.0–15.5	17	15	11	11	77	36
16.5–16.0	20	20	16	16	76	66
17.0–16.5	46	14	23	26	82	103
17.5–17.0	52	17	20	27	132	131
18.0–17.5	75	40	15	37	98	129
18.5–18.0	69	34	32	26	110	120
19.0–18.5	72	40	34	33	130	120
19.5–19.0	63	51	50	49	142	107
20.0–19.5	64	52	34	39	149	110
20.5–20.0	75	70	64	70	169	155
21.0–20.5	107	59	91	91	179	160
21.5–21.0	140	82	120	125	216	192
22.0–21.5	168	87	197	189	238	193
22.5–22.0	221	115	299	291	266	242
23.0–22.5	332	115	373	479	318	303
23.5–23.0	666	220	542	827	338	337
24.0–23.5	1129	498	683	1211	248	159

TABLE VIII(b). Differential star counts.

Plate J magnitude	2740	2741	2742	2743	2747	2766	12 plates
<13.0	5	5	0	4	6	3	53
13.5–13.0	0	6	2	0	2	2	30
14.0–13.5	2	3	2	3	4	0	53
14.5–14.0	5	8	2	3	3	8	71
15.0–14.5	14	12	4	5	11	4	127
15.5–15.0	20	17	12	17	8	13	189
16.0–15.5	28	26	8	28	11	12	280
16.5–16.0	35	21	24	37	20	17	368
17.0–16.5	37	27	30	52	18	17	475
17.5–17.0	31	30	28	63	39	32	602
18.0–17.5	31	24	32	93	23	32	629
18.5–18.0	39	40	28	65	27	36	626
19.0–18.5	37	44	27	60	29	34	660
19.5–19.0	61	55	30	75	33	33	749
20.0–19.5	49	51	37	79	56	41	761
20.5–20.0	71	80	65	112	57	32	1020
21.0–20.5	88	86	61	116	51	55	1144
21.5–21.0	89	100	76	126	84	59	1409
22.0–21.5	75	113	86	145	86	84	1661
22.5–22.0	117	118	102	135	96	114	2116
23.0–22.5	190	148	128	164	112	139	2801
23.5–23.0	244	235	268	150	197	209	4233
24.0–23.5	325	436	486	119	378	331	6003

ported in our earlier paper (Tyson and Jarvis 1979) are due to improvements in the classifier, additional photometric data, and additional fields. (We will report on the two-point clustering correlation functions in a separate paper.)

Stellar data for stars brighter than 21st mag are consistent with the van Rhijn luminosity function (Allen 1973) together with a simple exponential disk model. The stellar counts between $J = 20$ and $J = 23$ mag are in agreement with a reasonable halo and disk model (Valdes *et al.* 1981). The increasing excess from 23 to 24 mag could be faint red stars not accounted for in the van Rhijn function, misclassified galaxies, or QSO's. Additional number and color data as a function of latitude and longitude are necessary for an adequate analysis of the stellar counts in halo-disk galaxy models.

Our galaxy counts shown in Fig. 9 do not show the expected effects of the K-correction based on conventional galaxy spectra. Indeed, the counts appear linear in $\log N$ vs J over a wide range. Over the range $17 \leq J \leq 24$ mag, the number of galactic objects brighter than apparent magnitude J follows the relation $\log N = 0.443(\pm 0.020)J - 6.45$. This overall slope shows no significant variation from area to area. Tests show that in the range $J > 23$ mag, a maximum of $\approx 8\%$ of galaxies could be misclassified as stellar objects. In addition, some

stellar objects may be QSO's. If both of these estimated stellar contributions are added to the galaxy counts, a negligible change in the slope is made. It appears that K-corrections, evolutionary effects, and cosmology conspire to give a linear observed log$N$ vs apparent magnitude relationship. Recently, Kron (1980) has obtained differential number count data for faint objects from 21st to 24th mag in good agreement with our data after correcting for photometry noise rectification by rebinning of fainter objects.

VIII. DISCUSSION

The ability to detect objects down to a limiting apparent magnitude of $J = 24$ has been demonstrated. The ability to classify these dim images, a much more difficult task, is also claimed. Although evidence has been presented that the classifier works well, its optimality and accuracy have not been established. The computing resources required to create and analyze substantial catalogs (order of 10^5 objects) are modest. Implementation of this or a similar software on larger computing systems would clearly improve throughput or allow processing of larger images. With our current system, the 12-hr image to list reduction process limits the number of plates processed to at most one per day. While only one source of data has been processed by FOCAS, there is nothing in the system that limits processing of any similar images obtained in a digital form. Images from large-area CCD arrays are prime candidates for processing with FOCAS.

Atmospheric seeing is of paramount importance in determining both the classification and detection capabilities of FOCAS. The shape features C_2 and C_4 are very sensitive to seeing. If the seeing is interpreted as a Gaussian intensity profile for unresolved objects, then C_2 varies as the seeing disk diameter squared and C_4 varies as the fourth power. Since the total integrated luminosity is constant for a given object, the peak intensity will be reduced as the object is spread out. This decreases the detection sensitivity at faint magnitudes as well as increases the difficulty of distinguishing stars and galaxies. With 0.1-arcsec resolution, the wide-field camera of the Space Telescope, if applied to this detection and classification task, would be limited by integration time and readout noise to ≈27th mag for galaxies of ≈0.5-arcsec size. Even taking into account the $(1 + z)^{-4}$ relativistic decrease in surface brightness, depending on q_0, more apparent evolution may occur for galaxies in the 3-mag range from 24 to 27 than observed in the range of 21st to 24th apparent magnitude.

This paper documents the basic automatic plate processing system including classification. Further major additions to FOCAS will include the ability to merge the results of the same field made in two or more different colors. Although the exact methods have not been determined, when three colors are available, classification will be done in either a 9-dimensional space or one of 21 dimensions. Nine dimensions would represent the addition of two color differences to the basic shape discrimination features. Twenty-one dimensions would result from classifying three complete 7-parameter sets for each object, one from each of the three plates. Increasing the number of dimensions used by the classifier requires only increasing memory allocations, but not substantial reprogramming. In either case the geometric registration and comparisons needed to locate the images of the same object are straightforward. Much of the ambiguity and difficulty in classification should be removed by these additional data. Preliminary results obtained with three colors in two fields are encouraging.

Summarizing, we have implemented a system, FOCAS, for the detection and classification of objects down to a dim limit of 24th mag. A catalog of 86 000 objects has been assembled from 12 plates which is magnitude limited approximately 3 mag dimmer than any previous catalog.

We wish to thank R. Kron for the use of two plates, the use of his SA 57 catalog, stellar magnitude sequences for SA 57 and SA 68, and many helpful discussions. We have also benefited from discussions with W. A. Sebok, P. Schechter, and D. Wells.

APPENDIX: ZERO-REDSHIFT ISOPHOTAL CORRECTION

Our observed isophotal magnitudes of faint galaxies are affected not only by the K-correction but also by the galaxy outer isophote falling below our faint surface luminosity cutoff. We calculate here the size of the combined effect (Δm), which corresponds to the transformation from observed isophotal magnitude to zero-redshift isophotal magnitude. Although we shall do the calculation for spirals (using Freeman's law), the average Δm for all galaxies is probably not very different. The resulting zero-redshift isophotal magnitude is for all practical purposes equal to the total magnitude, since our surface luminosity detection threshold is sufficiently low to detect 25th-mag galaxies.

Using the notation of Tinsley (1976) and Petrosian (1976), the surface luminosity $\sigma_\nu(\theta_r,\nu,z)$ at projected angle θ_r, frequency ν, and redshift z is given by Weinberg (1972):

$$\sigma_\nu = B_\nu(\theta_r,\nu,t_0)k(z)E(z)(1+z)^{-4}, \qquad \text{(A1)}$$

with $E(z) = B_\nu(r,\nu,t)/B_\nu(r,\nu,t_0)$ (evolution) and $k(z) = B_\nu(r,\nu,t_0)(1+z)/B_\nu(r,\nu_0,t_0)$ (K-correction) and where B is the surface brightness of the galaxy. Similarly, the flux at luminosity distance D is given by

$$f_\nu(\theta,\nu,z) = \frac{L_\nu(r,\nu,t_0)}{4\pi D^2}k(z)E(z). \qquad \text{(A2)}$$

TABLE IX. Zero-redshift isophotal magnitude and K corrections.

Δm	z	K_j	$\langle J \rangle$
0.17	0.01	0.02	12.9
0.25	0.1	0.21	17.9
0.40	0.2	0.40	
0.60	0.3	0.57	
0.90	0.4	0.75	
1.34	0.5	0.9	
2.06	0.6	1.2	23.6

In our object detection search, we make a cutoff at surface brightness $\sigma_{\rm cutoff} = \alpha\sigma_{\rm sky}$ ($\alpha \approx 0.03$). Thus, from (A1) $B_\nu(r_c,\nu,t_0)k(z)E(z) = (1+z)^4\alpha\sigma_{\rm sky}$. Now assume Freeman's law (Freeman 1975) (since >70% of all galaxies are spirals): $B(r) = B_0\exp(-r/r_0)$, with $-2.5\log B_0 = 21.5$ mag/arcsec^2, which gives

$$B_0\exp(-r_c/r_0) = (1+z)^4\alpha\sigma_{\rm sky}/k(z)E(z), \quad \text{(A3)}$$

whence making the first-order approximations $E = 1$ and $-2.5\log k = 5\log(1+z)$, we find $\exp(-r_c/r_0) = (1+z)^6\alpha\sigma_{\rm sky}/B_0$, where $(\alpha\sigma_{\rm sky}/B_0) \approx 0.03$. Therefore

$$\left(\frac{r_c}{r_0}+1\right) = 4.51 - 6\log(1+z). \quad \text{(A4)}$$

The luminosity found out to the cutoff radius r_c is

$$L_\nu(r_c,\nu,t_0) = 2\pi\int_0^{r_c} B_\nu(x,\nu,t_0)x\,dx,$$

with $B_\nu(x) = B_0\exp(-x/r_0)$, giving

$$L_\nu(r_c) = 2\pi B_0 r_0^2\left[1 - e^{-r_c/r_0}\left(\frac{r_c}{r_0}+1\right)\right]. \quad \text{(A5)}$$

Thus $L_\nu(0) = 0$ and $L_\nu(\infty) = 2\pi B_0 r_0^2$. From (A3) and (A5), the lost luminosity is given by

$$\Delta l_{\rm lost} = 2\pi\alpha r_0^2(1+z)^4\sigma_{\rm sky}\left(\frac{r_c}{r_0}+1\right)\Big/k(z)E(z) \quad \text{(A6)}$$

or

$$\Delta l_{\rm lost} = l_\nu(\infty)\left(\frac{\alpha\sigma_{\rm sky}}{B_0}\right)(1+z)^4\left(\frac{r_c}{r_0}+1\right)\Big/{\rm k}(z)E(z). \quad \text{(A7)}$$

The lost apparent luminosity or flux is then

$$\Delta l_{\rm lost} = l\left(\frac{\alpha\sigma_{\rm sky}}{B_0}\right)(1+z)^6\left(\frac{r_c}{r_0}+1\right). \quad \text{(A8)}$$

Now, $\alpha\sigma_{\rm sky}/B_0 = 0.03$ and from (A4) the observed flux is

$$f_{\rm obs} = \int\left(\frac{L_\nu(\infty)}{4\pi D^2} - \Delta l_\nu\right)d\nu = l\left[1 - 0.03(1+z)^6\left(\frac{r_c}{r_0}+1\right)\right]. \quad \text{(A9)}$$

The corresponding observed magnitude is

$$m_{\rm obs} = -2.5\log l - 2.5\log\{1 - 0.03(1+z)^6 \times [4.51 - 6\ln(1+z)]\}. \quad \text{(A10)}$$

The magnitude correction $\Delta m = m_{\rm obs} - m$ is

$$\Delta m = -2.5\log\{1 - 0.03(1+z)^6 \times [4.51 - 6\ln(1+z)]\}. \quad \text{(A11)}$$

Note that Δm embodies both the K-correction and the isophotal correction. From this relation we calculate the magnitude corrections in Table IX as a function of redshift and we also show our estimate of the K-correction alone, K_J, and the average apparent magnitude, $\langle J \rangle$. Color gradients in galaxies will tend to raise this zero-redshift isophotal magnitude correction, since the core is red compared to the outer disk. An explicit gradient, if known, could be introduced in Eq. (A3). Finally, we have not made this Δm correction in any of our listed or plotted data.

REFERENCES

Allen, C. W. (1973). *Astrophysical Quantities* (Athlone, London).

Ball, G. H., and Ball, D. J. (1967). "A clustering technique for summarizing multivariate data," Behav. Sci. **12,** 153–156.

Batchelor, B. G. (1974). *Practical Approach to Pattern Classification* (Plenum, New York).

Benedict, G. F., and Shelus, P. J. (1979). "Applications of automated inventory techniques to astrometry," in *Modern Astrometry,* edited by F. V. Prochazka and R. H. Tucker (Vienna University Observatory, Vienna).

Chiu, G. (1976). "Scales and distortion coefficients of the Lick, KPNO, and Hale prime-focus correctors," Publ. Astron. Soc. Pac. **88,** 803–805.

Freeman, K. (1975). In *Galaxies and the Universe,* edited by A. Sandage, M. Sandage, and J. Kristian (University of Chicago, Chicago).

Herzog, A. D., and Illingworth G. (1977). "The structure of globular clusters. I. Direct plate automated reduction techniques," Astrophys. J. Suppl. **33,** 55–67.

Holmberg, E. (1975). "Magnitudes, colors, surface brightness, intensity distributions, absolute luminosity, and diameters of galaxies," in *Galaxies and the Universe,* edited by A. Sandage, M. Sandage, and J. Kristian (University of Chicago, Chicago).

Hu, M. (1962). "Visual pattern recognition by moment invariants," IRE Trans. Inf. Theory **TI-2,** 179–187.

Kendall, M. G., and Stuart, A. (1977). *The Advanced Theory of Statistics* (Charles Griffin, London).

Kibblewhite, E. J. (1975). "The design of the new S.R.C. automated photographic measuring system," in *Image Processing Techniques in Astronomy,* edited by C. de Jager and H. Nieuwenhuijzen (Reidel, Dordrecht), pp. 217–222.

Kron, R. G. (1979). Private communication.

Kron, R. G. (1980). "Photometry of a complete sample of faint galaxies," Astrophys. J. Suppl. **43,** 1.

Lorre, J. (1979). "Recent developments at JPL in the application of

image processing techniques in astronomy," Proc. SPIE **172,** 394–402 (Instrumentation in Astronomy III).
Oemler, A. (1976). "The structure of elliptical and cD galaxies," Astrophys. J. **209,** 693–709.
Petrosian, V. (1976). Astrophys. J. Lett. **209,** L1.
Pratt, N. M. (1975). "The COSMOS facility at the Royal Observatory Edinburgh," in *Image Processing Techniques in Astronomy,* edited by C. de Jager and H. Nieuwenhuijzen (Reidel, Dordrecht), pp. 217–222.
Ritchie, D. M., and Thompson, K. (1974). "The UNIX operating system," Commun. Assoc. Comput. Mach. **17,** 365–375.
Rosenfeld, A., and Kak, A. C. (1976). *Digital Picture Processing* (Academic, New York), pp. 296–302.
Sammon, J. W. (1969). "A nonlinear mapping for data structure analysis," IEEE Trans. Comput. **C-18,** 401–409.
Sandage, A. (1972). "The redshift-distance relation. III. Photometry and the Hubble diagram for radio sources and the possible turn-on time for QSO's," Astrophys. J. **178,** 25–44.
Sandage, A., Veron, P., and Wyndham, J. D. (1965). "Optical identification of new quasi-stellar radio sources," Astrophys. J. **142,** 1307–1311.
Saslaw, W. C., Tyson, J. A., and Crane, P. (1978). "Optical emission in the radio lobes of radiogalaxies," Astrophys. J. **222,** 435–439.
Schweizer, F. (1976). "Photometric studies of spiral structure. I," Astrophys. J. Suppl. **31,** 313–332.
Sebok, W. L. (1979). "Optimal classification of images into stars or galaxies—a Baysean approach," Astron. J. **84,** 1526–1536.
Tinsley, B. (1976). Astrophys. J. Lett. **210,** L49.
Tsubaki, T., and Engvold, O. (1975). "An analytic representation for photographic characteristic curves," AAS Photobull. **9,** 17–19.
Tyson, J. A. (1979). KPNO 2.1-m photometer.
Tyson, J. A., and Jarvis, J. F. (1979). "Evolution of galaxies: Automated faint object counts to 24th magnitude," Astrophys. J. Lett. **230,** 153–156.
Valdes, F., Jarvis, J. F., and Tyson, J. A. (1981). To be published.
Weinberg, S. (1972). *Gravitation and Cosmology* (Wiley, New York).